IEEE Access
Multidisciplinary | Rapid Review | Open Access Journal

Received January 25, 2021, accepted January 31, 2021, date of publication February 2, 2021, date of current version February 9, 2021.

Digital Object Identifier 10.1109/ACCESS.2021.3056589

Reduction of Torque Ripples in Multi-Stack Slotless Axial Flux Machine by Using Right Angled Trapezoidal Permanent Magnet

MUHAMMAD YOUSUF[1], FAISAL KHAN[1], (Member, IEEE), JUNAID IKRAM[2], RABIAH BADAR[2], SYED SABIR HUSSAIN BUKHARI[3,4], (Member, IEEE), AND JONG-SUK RO[4]

[1]Department of Electrical and Computer Engineering, COMSATS University Islamabad, Abbottabad Campus, Abbottabad 22060, Pakistan
[2]Department of Electrical and Computer Engineering, COMSATS University Islamabad, Abbottabad 22060, Pakistan
[3]Department of Electrical Engineering, Sukkur IBA University, Sukkur 65200, Pakistan
[4]School of Electrical and Electronics Engineering, Chung-Ang University, Seoul 156-756, South Korea

Corresponding author: Jong-Suk Ro (jongsukro@gmail.com)

This work was supported and conducted under the Competency Development Program for Industry Specialists of the Korean Ministry of Trade, Industry and Energy (MOTIE), operated by the Korea Institute for Advancement of Technology (KIAT) (HRD Program for Industrial Convergence of Wearable Smart Devices), under Grant P0002397, and in part by the Brain Pool Program through the National Research Foundation of Korea (NRF) funded by the Ministry of Science and ICT under Grant 2019H1D3A1A01102988.

ABSTRACT The aim of this paper is to design, analyze and optimize the ''Multi-Stack Slotless Axial Flux Switching Permanent Magnet Machine''. In the design process, mathematical models are implemented, and the Finite Element Method (FEM) is performed to analyze the machine performances. The paper aims to minimize the occurrence of cogging torque and torque ripple in the multi-stack slotless stator AFPM machine. As a consequence, it reduces the vibrations in the machine and increases its life span. Multi-stack slotless stator AFPM machine with a right-angled trapezoid-shaped PM is proposed and comparison is done with conventional shape AFPM machine. In order to examine the performance of multi-stack slotless stator AFPM machine Finite Element Analysis (FEA) is used. To further enhance the characteristics of the designed machine with the proposed right-angled PM shape, optimization is done by considering inner and outer pole pitch as the design variables. In optimization process, krigging method assigned with Latin Hyper-cube Sampling and a genetic algorithm (GA) is performed due to suitability with non-linear data. Then, finite element analysis by JMAG-Designer is performed to verify the results. It is determined that optimized model has achieved 65% reduction in torque ripples as compared with the conventional design. Hence, this work attempts to optimize the performance of the AFPM machine.

INDEX TERMS Axial flux machine, torque ripples, cogging torque, slotless stator, finite element analysis.

I. INTRODUCTION

Permanent magnet machines have a wide range of use in the electric vehicle and aerospace industries all around the world providing the exceptional performances such as high reliability, high-power density, and high efficiency [1]–[4]. Axial flux permanent magnet (AFPM) machines are installed for various applications because of their benefits [5]–[9]. Two main applications of AFPM machines are for renewable energy-based production of electricity [10], [11] as well as the application for electric and hybrid vehicles [6], [12]. Axial flux permanent magnet machine has a wide range of benefits such as greater power-to-weight ratio and requires less amount of core material due to its compact design. As compared to the conventional machines, the level of noise and vibration is lesser because of its high efficiency, short length to radius ratio and high torque density [13]. Multi-stack slotless stator AFPM machine provides smooth operation of the machine due to elimination of stator core losses and less cogging torque. The slotless design solves a big issue in the construction of machines that is the slotting of the stator and it also reduces the cost of the machine.

In this research multi-stack, slotless stator AFPM machine is investigated. It is convenient to discuss it as a concept rather than a machine type. To fulfill the necessity of the application, we can place rotors and stators alternatively, hence obtaining

The associate editor coordinating the review of this manuscript and approving it for publication was Fabio Massaro.

a multistage machine. Modularity is an interesting feature that can be obtained using this arrangement. Windings in different stages can be attached either in parallel or series. Relying upon the momentary requirement of the application, the stages can be connected or disconnected. This will allow the machine to tolerate even in case of any fault by disconnecting any malfunctioning stages [14].

Torque ripple must be reduced for the smooth operation of the multi-stack slotless stator AFPM machine. However, the multi-stack slotless stator AFPM machine also generates torque ripple similar to the other types of PM machines. Torque ripple is produced in multi-stack slotless stator AFPM machine due to cogging torque, magnetic circuit saturation, and non-sinusoidal back EMF. Geometric parameters can be upgraded to decrease the torque ripple such as skewing the rotor or stator, variation of slot opening, special shapes of slots, a proper slot-pole number combination, using fractional slot windings, the variation of the magnet width, magnets mounted in trapezoid shape configurations, pole-arc to pole-pitch ratio optimization, creating slotless configurations [15].

The high speed AFPM machine has also a great potential in various fields such as turbo-compressors, machine spindles and fly wheel [16]–[18]. AFPM machines designed for ultra-high-speed applications required the reduced torque ripples and losses to ensure the high performance and smooth operation. In [19], AFPM generator aiming at the rated speed of 1000000 rpm is developed and the toroidal winding is used to reduce the torque ripples and a novel PM shape is proposed to achieve the sinusoidal back EMF and an experimental validation of the generator at 32000 rpm is carried out in [20]. In [21], the winding configurations analysis for high speed AFPM machines are discussed and comparison for different winding configurations are also made.

The magnetic bridges that are equivalent to fan shaped saturation regions and the simplified trapezoid magnet is implemented to obtain the accurate prediction in [22], [23]. In [24], two novel hybrid PM machines are presented to enhance the torque density. The peak-to-peak torque density for short duration operation is specifically considered. Optimization and electromagnetic performance comparison are also carried out for the proposed and conventional machines models.

For an AFPM machine, the ratio of torque ripple to average torque has been reduced in [25]. A design procedure based on sets of levels was employed to obtain a design of optimal stator of Internal Permanent Magnet (IPM) machine to minimize torque ripple in [26]. The maximization of torque to weight ratio in permanent magnet synchronous machines has been studied in [27] by using topology optimization. A decrease in torque ripple and cogging torque, eddy current losses in the teeth of the stator, and therefore enhanced performance and efficiency of the AFPM machines is estimated with a suitable magnet shape [28], [29]. A trapezoidal shape is better than a rectangular or circular shape due to the more effective utilization of rotor surface area [30].

Cogging torque can be eliminated by maintaining the air-gap reluctance to be fixed corresponding to the position of the rotor [31]. In this research, a right-angled trapezoid-shaped permanent magnet having two angles of 90 degrees is proposed for the quality enhancement of the output torque and it also reduces the torque ripples due to reduced air gap reluctance variations in the proposed magnet shape. Performance of multi-stack slotless stator AFPM machine is carried out by using proposed right-angled trapezoid-shaped magnet and comparison is done with conventional magnet shape. Torque ripple, cogging torque, and harmonics in back EMF are reduced by using the proposed right-angled trapezoid-shaped magnet and are compared to the conventional magnet shape by using 3D FEA. It is revealed that cogging torque and torque ripple are decreased in the proposed model as compared to the conventional model. The proposed magnet shape is optimized to further increase the designed machine performance. The Latin Hyper Cube Sampling (LHS) is employed to obtain the appropriate number of samples of design variables. Then for the approximation of the objective function Kriging method is utilized and finally optimal results are obtained by using the Genetic Algorithm (GA). Inner and outer pole arc to the pole pitch ratios is taken as a design variable. For the entire optimization process, the volume of the permanent magnets is remained fixed for all the samples as of the conventional shape magnet. The torque quality in consort with average output torque is improved in the optimized model. Hence, this research attempts to optimize the performance of the AFPM machine. The research methodology is represented in Fig. 1.

This research paper is classified in to VI sections. Section II describes the comparison of conventional and proposed model. This section also discussed the conventional design process, propose magnet shape and electromagnetic performance comparison in detail. In Section III, the optimization process is presented and briefly explained. In section IV, convergence progress analysis is made to describe the influence of the parameter with respect to the objective functions. In Section V, evaluation and comparisons of electromagnetic performances are carried out for the optimized model. Finally, the conclusion is made in Section VI.

II. COMPARISON OF CONVENTIONAL AND PROPOSED MODEL

The design process of the multi-stack slotless stator AFPM machine, proposed magnet shape, and performance comparison of conventional with proposed models are examined in this section. Multi-stack slotless stator AFPM machine with a trapezoidal magnet is known as conventional model however right-angled trapezoid shape magnet is known as the proposed model.

A. DESIGN PROCESS

A 12 kW three-phase multi-stack slotless stator AFPM machine is presented in this paper. Conventional multi-stack slotless stator AFPM machine has a trapezoidal magnet shape. The machine has three-disc type rotors and two slotless

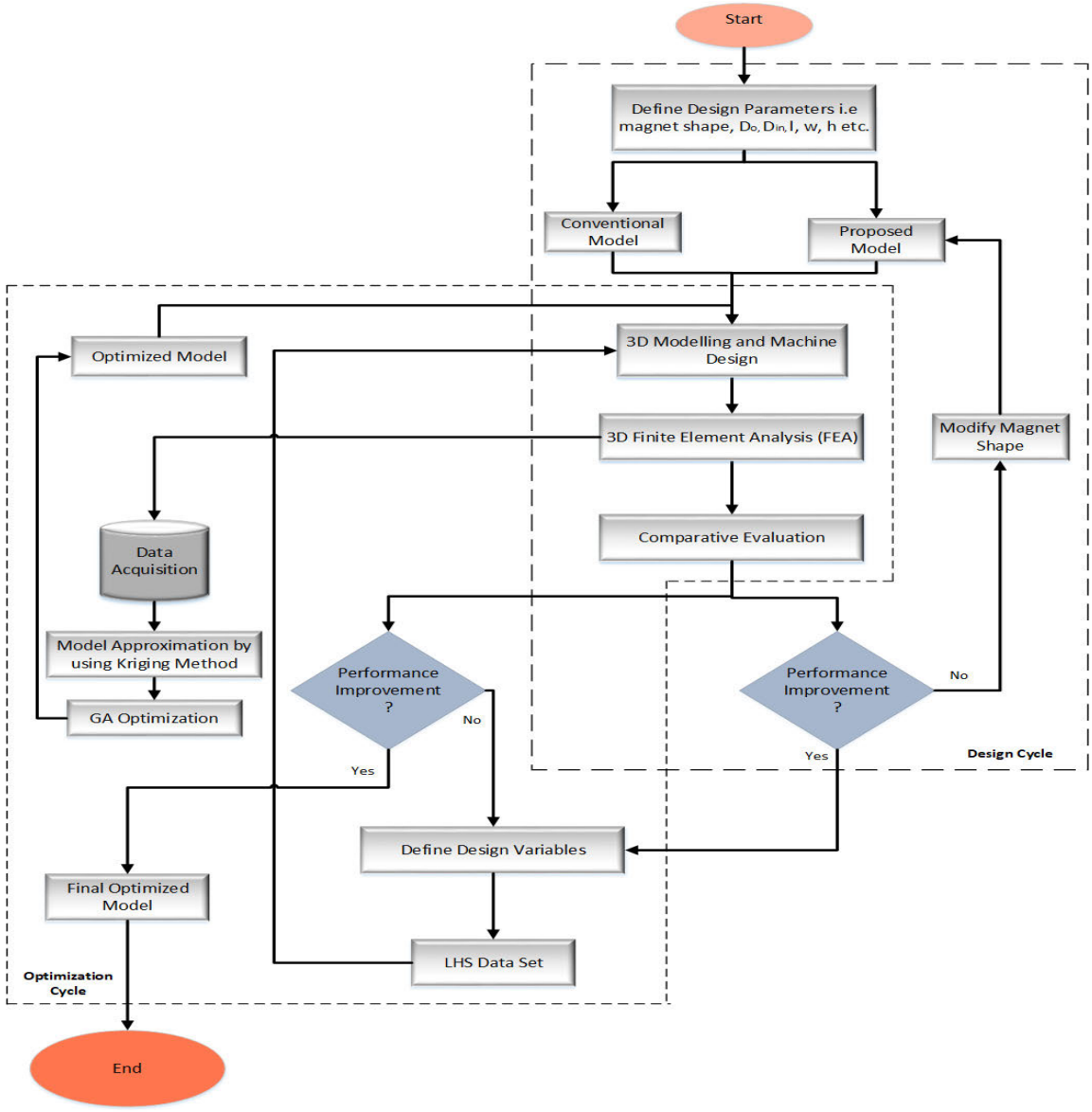

FIGURE 1. Flow chart of the design process.

iron-cored stators. Rotors have disc yoke with PMs placed on its surface, drum winding is on stator and stator consists of twenty-four coils. The trapezoidal-shaped coil is chosen to enhance the effective utilization of the stator core. No particular application is directed, and so no specific constraints are employed on machine smartness. But necessities like large force density and mechanical strength (that put on generally to a lot of business and traction applications) still must be satisfied. Therefore, a 12 kW multi-stack slotless stator AFPM machine is designed with the toroidal winding of trapezoidal shape is used in stator due to its greater output torque capability. Since the standard speed is set to 800 rpm, the output torque of the machine is 170 Nm. The outer radius of the stator is set to148 mm and the inner radius is set to 100 mm so that the active length of the winding is 48 mm. SPP = 2/5 is chosen due to the increased standard winding factor (0.966) of all possible values. Using 24 stator coils and 10 pole pairs, the frequency is set to 133.3 Hz and each coil has 18 no. of turns.

The conventional AFPM machine represented in Fig. 2 are referred to as the basic model in this paper. Basic model has simple structure that is compatible with its commercial use in wind power generation and other low-cost applications. On each rotor disk, 20 Nd-Fe-B surface-mounted permanent magnets are used. The permanent magnet has an average width of 29 mm that corresponds to around 74 % of the pole. The 2mm air gap is selected in this AFPM machine. The height of the permanent magnet is fixed to 5 mm. Multi-stack slotless stator AFPM machine is affected by the dimension and the stator material and rotor core. The rotor and stator with steel material have comparatively greater axial force as compared to a non-magnetic material [32]. The rotor core is made of steel material. The entire axial length of the machine comprising both air gaps is 86 mm. Table 1 sums up the

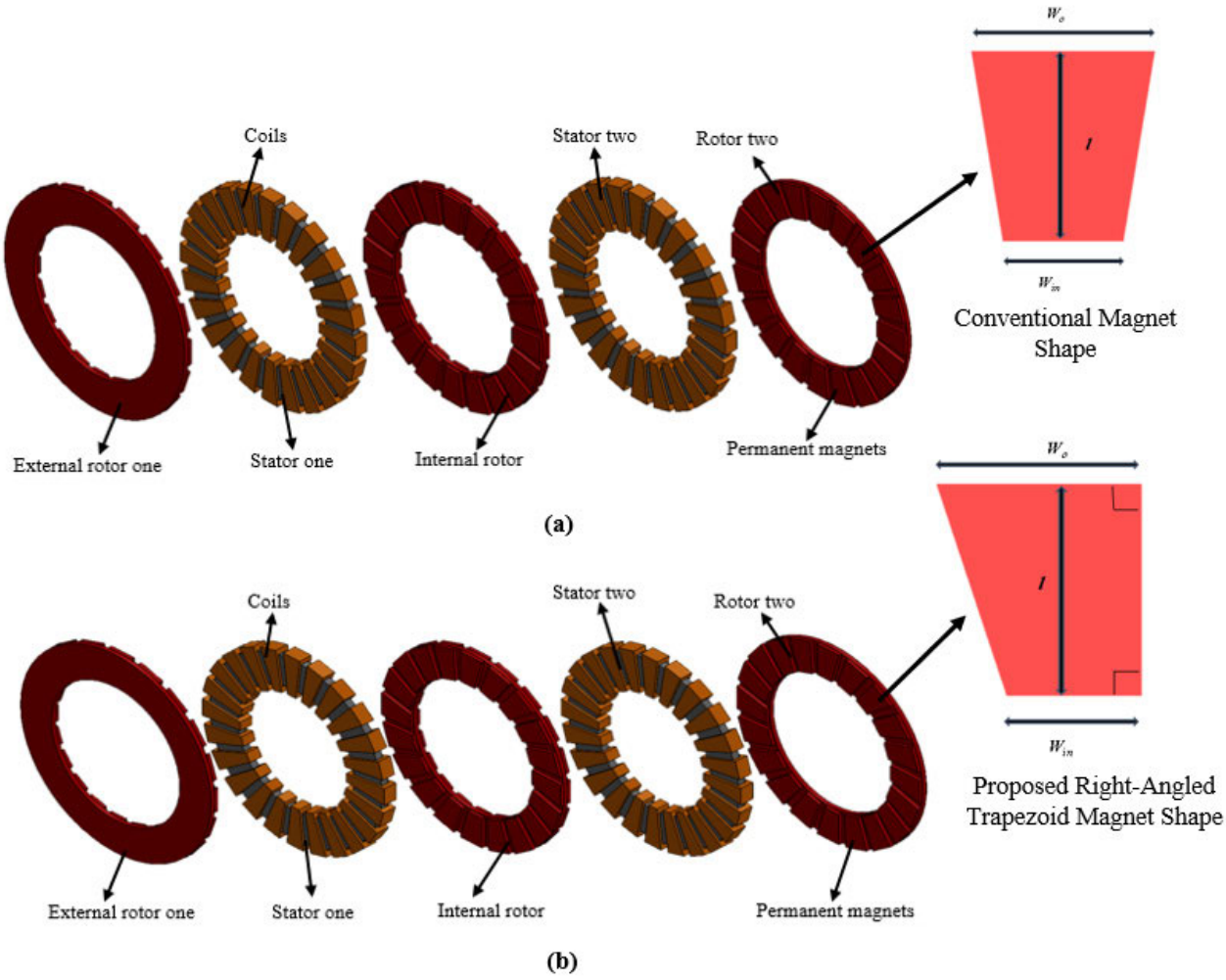

FIGURE 2. Multi-stack slotless AFPM machine (a) conventional, and (b) proposed models.

various design parameters values of the multi-stack slotless stator AFPM machine. The design process of the basic model is briefly discussed mathematically as in [33]. The input power can be calculated as:

$$P_{in} = 2\frac{m}{T}\int_0^T E_m \sin(\omega t) I_m \sin(\omega t) dt \tag{1}$$

In (1), m represents the phase number, E_m denotes the back EMF amplitude and I_m depicts the current respectively and the output power is illustrated as:

$$P_{out} = \gamma m E_m I_m \tag{2}$$

where γ represents efficiency. The flux computations can be made by using the (3).

$$\varphi = \varphi_m \cos(N_p \alpha_r) \tag{3}$$

where φ, α_r and N_p represents the flux magnitude, the rotor position and rotor pole numbers, respectively. The back EMF can be computed as in (4)

$$e(t) = N_{ph}\omega_r N_P \varphi_m \sin(N_p \alpha_r) \tag{4}$$

where, N_{ph} represents the phase coil turns and ω_r denotes the rotor angular speed, respectively. substituting (3) in (4), back EMF can be represented as:

$$e(t) = N_{ph}\omega_r N_P k_d k_f B_g \alpha_i \frac{1}{N_s}\frac{\pi}{4}(D_{out}^2 - D_{in}^2) \tag{5}$$

where, $B_g, k_d, k_f, \alpha_i$and N_s represents the air gap flux density, lux leakage coefficient, airgap flux density coefficient, pole arc coefficient and slot numbers, respectively. D_{in} and D_{out} depicts the inner and outer diameter of the stator and rotor, respectively.

The armature current can also be determined as in (6).

$$I_m = \frac{\sqrt{2} A_e \pi D_{in}}{2 m N_{ph}} \tag{6}$$

where A_e represents the electrical loading. Substituting (5), (6) and in (2) give rise to:

$$P_{in} = \frac{\sqrt{2\pi^3}}{240}\frac{N_p}{N_s} k_d k_f k_{io}(1 - k_{io}^2) A_e B_g \alpha_i D_{out}^3 n_{rpm} \gamma \tag{7}$$

TABLE 1. Design parameters of conventional multi-stack AFPM machine model.

Parameters	Values	Parameters	Values
Outer diameter	296 mm	No of coils	24
Inner diameter	200 mm	Turns per coil	18
Height of rotor iron core	6 mm	Magnet Volume	6790.35 mm^3
Height of stator iron core	11 mm	Air gap	2 mm
Height of Magnet	5 mm	Outer width of magnet	35 mm
Length of Magnet	46.83 mm	Inner width of magnet	23 mm
Average Width of Magnet	29 mm	Coil height	7 mm
Speed	800 rpm	Coil width	20 mm
No of poles	20	Frequency	133.34 Hz

where k_{io} and n_{rpm} shows the inner to outer diameter ratio and rotor speed in rpm, respectively. Further the output torque can be determined as in (7).

$$T_{out} = \frac{\sqrt{2}}{240}\pi^2 \frac{N_P}{N_s} k_d k_f k_{io}(1 - k_{io}^2) A_e B_g \alpha_i D_{out}^3 \gamma \tag{8}$$

It can be clearly seen from (7) and (8), the power and torque are directly related to B_g, A_e and N_p/N_s.

From (7), the outer diameter is given as in (9).

$$D_{out} = \sqrt[3]{\frac{240 P_{out} N_s}{\sqrt{2}\pi^3 N_r k_d k_f k_{io}(1 - k_{io}^2) A_e B_g \alpha_i n_{rpm} \gamma}} \tag{9}$$

B. PROPOSED MAGNET SHAPE

The cogging torque is an undesirable phenomenon that happens as a result of a change in reluctance between the rotor poles and the stator teeth. Alternatively stated, it is due to the interaction between the magnetic flux and the stator reluctance change due to stator slots.

$$T_{cogg} = -\frac{1}{2}\phi_{gap}^2 \frac{dR}{d\theta} \tag{10}$$

where ϕ_{gap} represents air gap magnetic flux and R represents the air gap reluctance. The equation (10) shows that flux or reluctance variations should be reduced to minimize cogging torque. However, reducing the flux reduces machine power and is not an effective way to minimize cogging torque. Hence, less variation in reluctance is an appropriate way to decrease the cogging torque. This variation can be reduced to some extent by shaping magnets. The proposed right-angled trapezoid shape magnet helps to minimize this variation and therefore cogging torque reduces.

Conventional trapezoidal magnet shape has slopes along both sides and uniform interpolar separation. However, the right-angled trapezoid-shaped permanent magnet has two angles of 90 degrees due to these right angles one side of the proposed shape magnet is straight, and the other side has a lesser slope which adds the skew effect. Furthermore, this shape also produces an unequal interpolar separation between magnets. Other parameters i.e., machine axial length, permanent magnet height, permanent magnet volume, rotor outer diameter, rotor inner diameter, etc. of the right-angled trapezoid shape magnet multi-stack slotless AFPM machine are the same as in the conventional shape permanent magnet multi-stack slotless AFPM machine. Both shapes are shown in Fig. 2.

The conventional trapezoidal shape magnet has more overall interaction between stator and PM of the rotor as compared to the proposed right-angled trapezoid shape PM due to constant interpolar separation. Proposed shape PM has a lesser slope and unequal interpolar separation due to which it has less overall interaction between stator and PM of the rotor. This less interaction between stator and PM of the rotor is also a cause of reduced cogging torque in the proposed model of multi-stack slotless AFPM machine.

The magnet's volume is kept constant. The right-angled trapezoid-shaped magnet volume is held constant as that of the conventionally shaped magnet by adjusting the length (l) of the right-angled trapezoid-shaped PM. The variables W_o, W_{in}, l, and h in Fig. 2 denote the trapezoid

outer width, trapezoid inner width, length, and height of the trapezoid, respectively. The volume of the right-angled trapezoid-shaped PM is given in eq. (11).

$$V_t = \frac{W_o + W_{in}}{2} lh \tag{11}$$

Airgap variations, unequal interpolar separation, skewing, notching, rotor pole-pairing and optimization are the techniques discussed in literature to reduce the cogging torque. Apart from recent efforts made to reduce the torque ripples, the average torque reduction is inevitable regardless the choice of either pole shaping or skewing [34]. This paper achieves a very low torque ripples with a minimum decrease in average torque by using a right-angled trapezoidal magnet shape. Conventional magnet shape is slightly modified to combine the effects of cogging torque reduction approaches specifically unequal interpolar separation, airgap variations and skewing to achieve the better output performances. The proposed design performance illustrates the effectiveness of the proposed magnet shape and its capability to reduce the torque ripples. After that optimization is carried out to achieve the better average output torque and eliminate the loss of average torque. Finally, optimized model with proposed magnet shape achieved the 65% torque ripple reduction while the increase in average output torque was 2.501Nm. Hence this work makes a significant contribution in the existing literature.

C. PERFORMANCE COMPERISON OF SLOTLESS MULTI-STACK AFPM MACHINE CONVENTIONAL AND PROPOSED MODELS COMPARISON

Results of conventional and proposed right-angled trapezoid PM model from 3D finite element analysis (FEA) are discussed in detail in this section. The right-angled trapezoid-shaped magnet is proposed that has a lower cogging torque than the conventional magnet shape. In addition, the proposed right-angled trapezoid-shaped magnet has better output torque quality and back EMF than the conventional magnet shape due to less reluctance variation and skew effect.

Flux density comparison in the air gap for conventional and proposed models is presented in Fig. 3. The figure displays that air gap flux density is almost the same for both the models because of no change in air gap length for both the models. To minimize the cogging torque and torque ripple reluctance variation approach is used and the air gap length is kept constant. The peak-to-peak air gap flux density value for both models is 0.92 T.

The plots of the flux density distribution of the conventional model in the coil region and the overall AFPM machine are represented in Fig. 4(a) and Fig. 4(b), correspondingly. The plots of flux density distribution of the proposed model in the coil region and the overall AFPM machine are represented in Fig. 5(a) and Fig. 5(b), correspondingly. Highest flux density (2.2 T) happens at the rotor core and is almost the same for both models. Highest flux density is observed to inspect the saturation of the rotor core. The coil region has

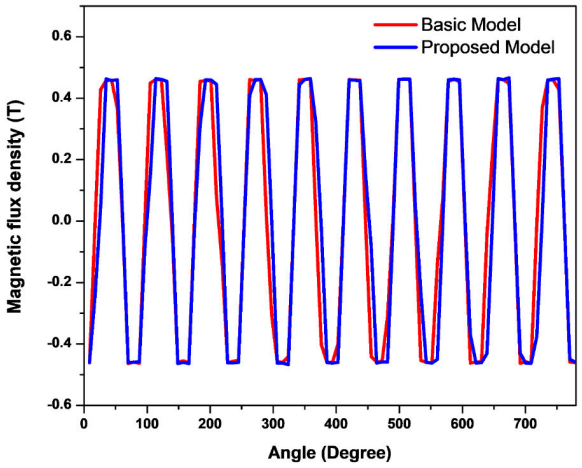

FIGURE 3. Comparison of air gap flux density of conventional and proposed models.

a highest flux density value of 0.6 T which is the same for both models.

The back EMF waveform of proposed and conventional models is represented in Fig. 6. The reduction in the proposed model back EMF is 3.26 V as compared to the conventional model. A considerable reduction in cogging torque is observed with the proposed model as compared to the conventional design. The minimum loss in back EMF of the proposed model is compromised due to the most significant cogging torque reduction simultaneously.

The fundamental harmonic component magnitude of the conventional and proposed model back EMF are 136 and 129, respectively. The conventional model has THD of 0.4704 % in back EMF and the proposed model has 0.4609 %. A decrease in THD from 0.4704 to 0.4609 is attained through the proposed model. The proposed model has enhanced fundamental harmonic component and reduced back EMF THD as compared to the conventional model due to its more sinusoidal flux density distribution. Back EMF THD of proposed and conventional models are presented in Fig. 7.

The cogging torque of the proposed and conventional model is given in Fig. 8. Cogging torque is reduced in the proposed model due to the change in PM shape. The proposed right-angled shape magnet has less reluctance variations due to which reduction in cogging torque is 47.32 %. Torque ripple is also decreased in the proposed model and the reduction in torque ripple is attained by reduction in cogging torque.

The output torque is obtained by connecting a load resistor of 1.2 ohms across each phase. The resistive load has a constant value i.e., 1.2 ohms for comparison of both the models because the rated current of conventional provides 3 Arms rated current at this value. The output torque of the proposed and conventional model is displayed in Fig. 9. The output torque of the conventional model is to somewhat increased, but the torque ripple is 8 %. There is a bit of reduction in the proposed model output torque and ripples in the proposed model is 4.16 %. There is 48 % reduction in torque ripple

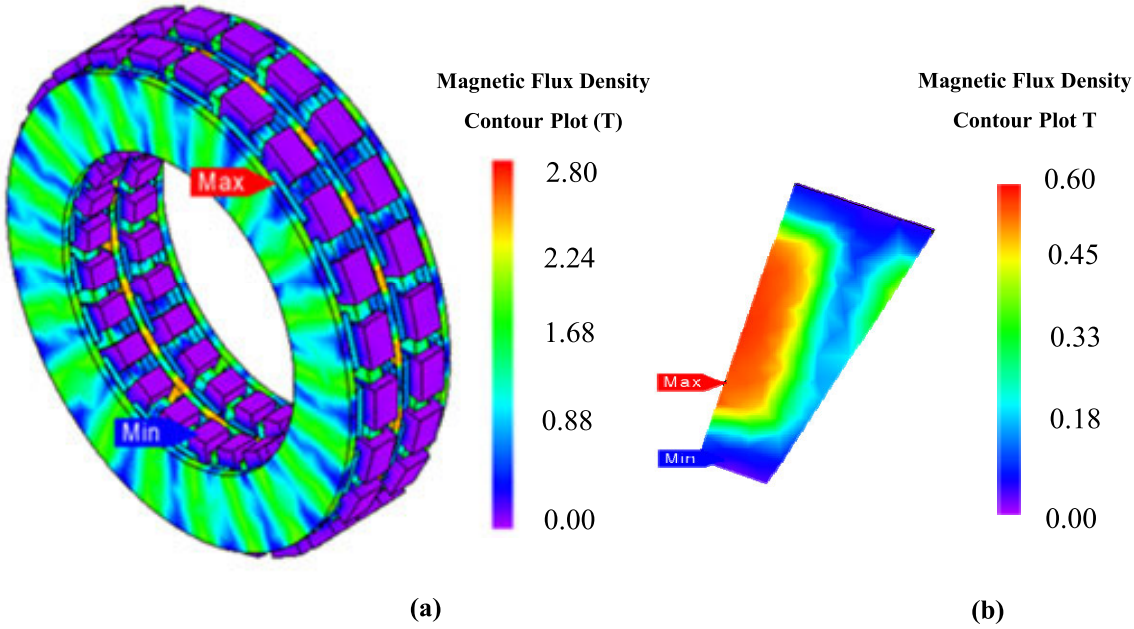

FIGURE 4. Flux density distribution of conventional model: (a) overall model (b) coil region.

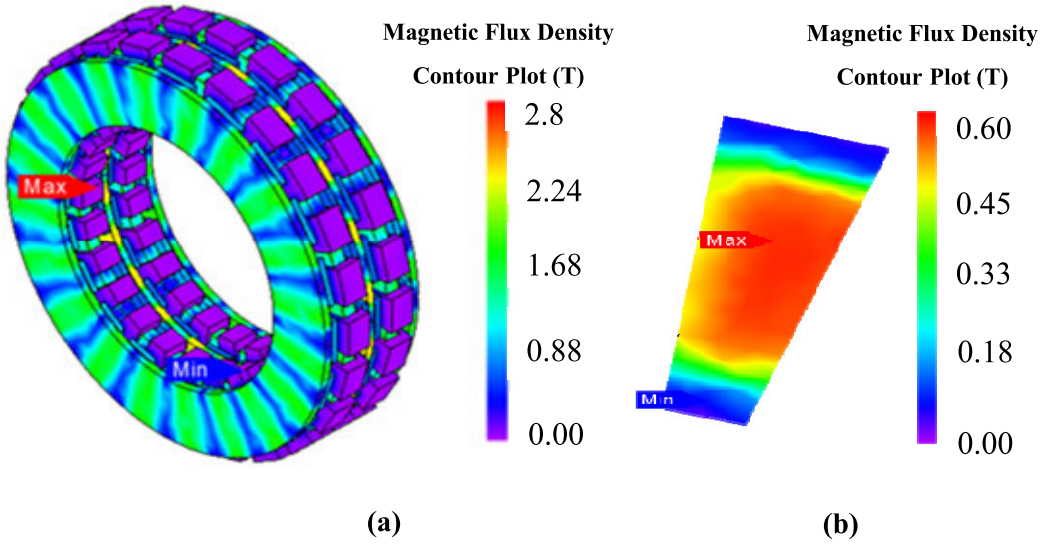

FIGURE 5. Flux density distribution of proposed model: (a) overall model (b) coil region.

in proposed model which is achieved by the reduction in cogging torque.

Performance comparison of proposed and conventional model is given in Table 2. The table shows the conventional model gives less $\tau_{cogging}$ and reduced torque ripples. There is a reduction in V_{rms} and output torque of the proposed model. Therefore, optimization of the proposed model is implemented to obtain the V_{rms} and output torque better than that of the conventional model in the next section.

III. PROPOSED MODEL OPTIMIZATION

In this section, proposed model optimization is implemented to enhance the output torque and torque quality as compared to the proposed model. The selection of the design variables and optimization process is explained briefly in this section.

A. DESIGN VARIABLES SELECTION

So as to build up an optimized model, pole arc to pole pitch ratio of the magnet towards external diameter α_{out} and pole arc to pole pitch ratio of the magnet toward internal diameter α_{in} were the parameters to optimized, with the objectives of increased back EMF and refining the feature of the output torque i.e., decreasing the torque ripple. The α_{out} and α_{in} are selected as designed variables as shown in Fig. 10. Limitations on the variable are mentioned below. By changing these dimensions of the permanent magnet between these limits the general structure of the PM shape will be the

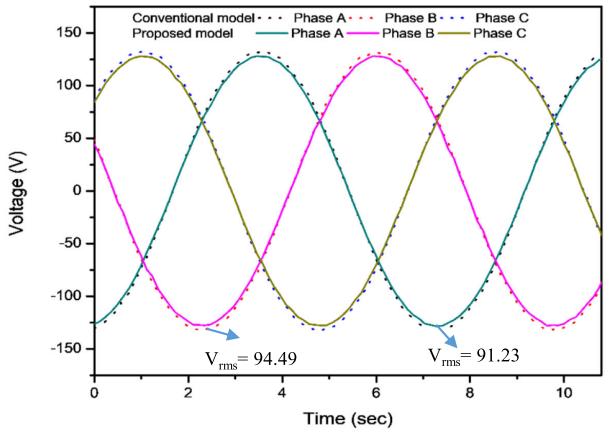

FIGURE 6. Comparison of back EMF of conventional and proposed models.

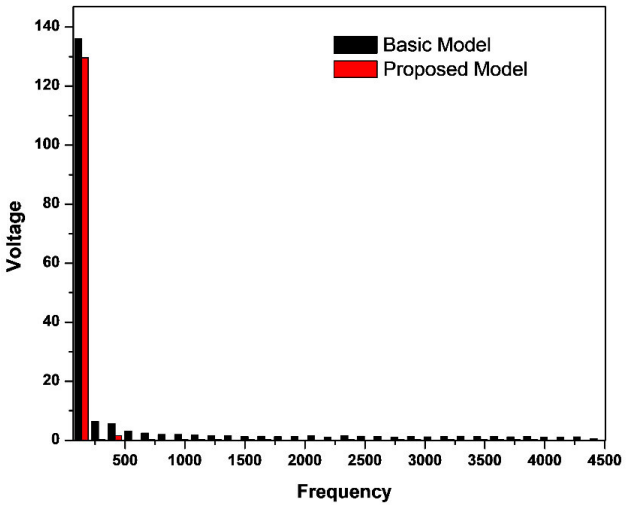

FIGURE 7. Comparison of harmonics of conventional and proposed models.

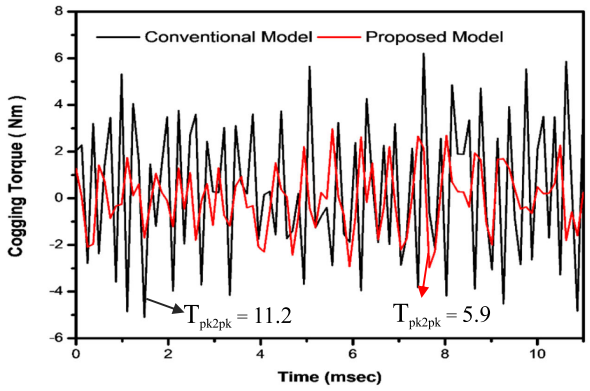

FIGURE 8. Cogging torque comparison of conventional and proposed models.

same as compared to the proposed shape. The volume of the right-angled trapezoid magnet shape is kept constant for each of the combination. It is an acknowledged circumstance that

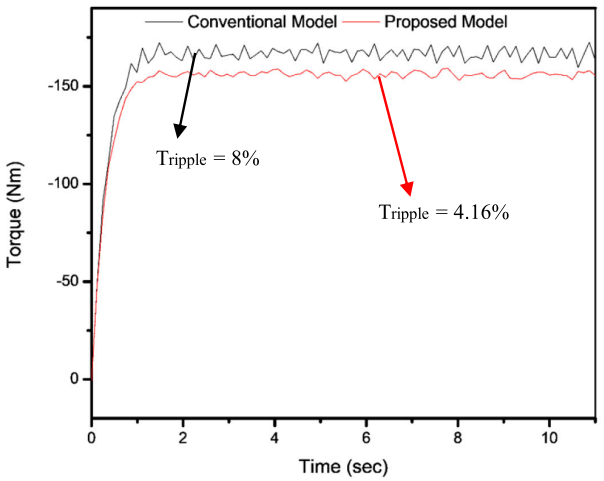

FIGURE 9. Torque comparison of conventional and proposed models.

the magnet pole arc has a great influence on the magnitude of the cogging torque [31].

The design variables X_1 and X_2 are the widths of the magnet toward the outer diameter of the rotor core and towards the inner diameter of the rotor core, respectively. By varying these lengths in the permissible limits i.e., $23.24 < X_1 > 42$ and $15.707 < X_2 > 28.5$, design variables samples are obtained by LHS.

B. OPTIMIZATION PROCESS

At first, the selection process of the objective function and design variables is completed. After that, the Latin Hypercube Sampling (LHS) technique is applied to plan the tests. From that point forward, the Kriging technique is utilized to estimate the objective function and afterward genetic algorithm (GA) was performed to determine optimum results for the chosen design parameters. At last, transient 3D FEA is implemented to check the output results in the optimized multi-stack slotless AFPM machine. The optimization procedure utilizing kriging and GA can be abridged as roughly in five stages and optimization process is described in the optimization cycle of the Fig. 1.

Stage 1: Define the objective function and determine the design variables.

Stage 2: Generate 20 introductory testing points in the entire design space by Latin hyper cube sampling (LHS) and compute their related objective values by 3-D FEA.

Stage 3: Estimated the model by kriging investigation based on LHS in PIAnO software by PIDOTEC Inc. [35].

Stage 4: Hunt the optimum value utilizing the genetic algorithm. Fitness modeling function F(i) of GA is illustrated as in [36]

$$F(i) = f(i) + \varepsilon P(i) \tag{12}$$

where $f(i)$ is the multi-objective function, i is the vector design variables, $P(i)$ represents the penalty function and ε depicts the penalty coefficient.

TABLE 2. Performance comparison of the conventional and proposed multi-stack AFPM machine models.

Parameters	Conventional Model	Proposed Model
V_{rms}	94.49	91.23
$\tau_{cogging}$ (peak-peak)	11.2	5.9
Average Torque	161.99	151.74
Torque Ripple	8 %	4.16 %
B_g (peak-peak)	0.92	0.92
VTHD	0.4704 %	0.4609 %

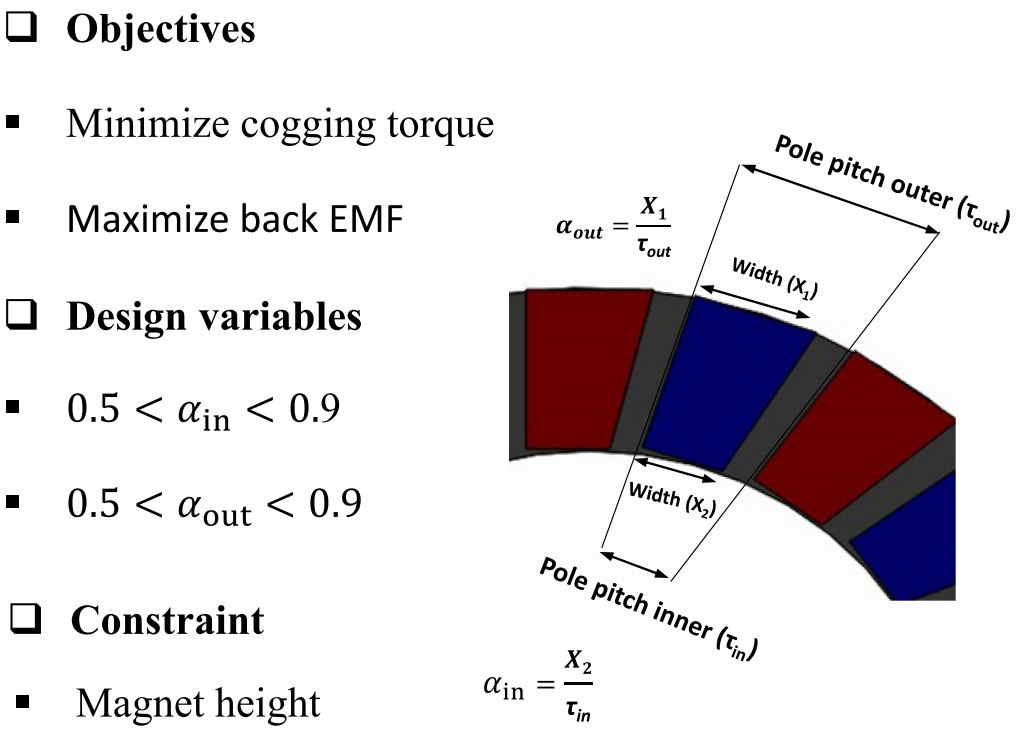

FIGURE 10. Design variables, objective functions and constraints.

Stage 5: If the model satisfies the optimization criteria then ends the process. If it does not satisfy the optimization criteria, then again adjust the design variables, and go to the *stage 2*.

IV. CONVERGENCE PROGRESS ANALYSIS FOR DESIGN VARIABLES AND OBJECTIVE FUNCTIONS

Optimal values of variables as per objective functions is achieved. The convergence progress analysis for the variables is represented in Fig. 11. The achieved optimal values for the design variables (X1, X2) were 33.117mm and 17.728, respectively. the enhancement in Back EMF and reduction in cogging torque is chosen as the objective functions as shown in Fig. 10. Cogging torque significantly affects the occurrence of vibration and noise in the machine and results in the torque ripples. Hence, it is required to minimize it as much as possible at the design stage. Torque ripple is related to the back EMF harmonics, must require to be minimized as much as possible because it enhances the vibration and noise in the machine [37]. The convergence results for the objective functions are depicted in Fig. 12 and Fig. 13, respectively. The determined cogging torque and

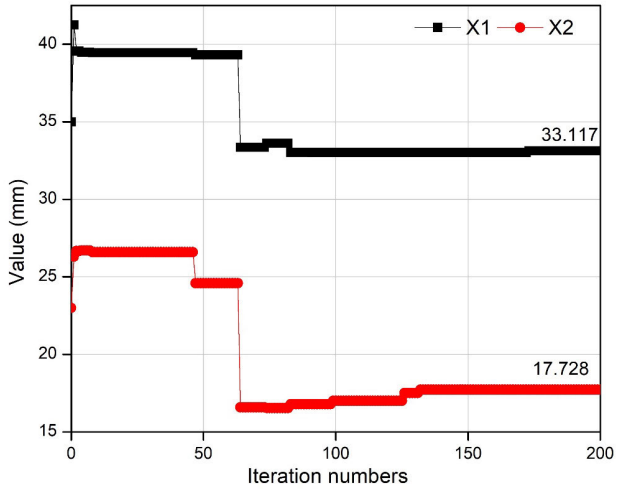

FIGURE 11. Convergence process of design variables.

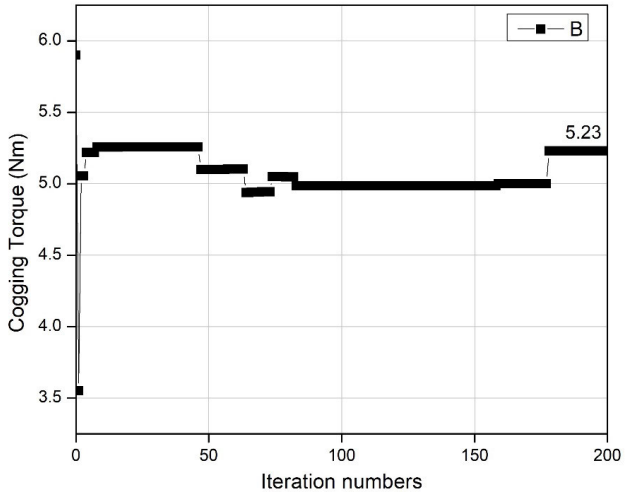

FIGURE 12. Convergence process of objective function (cogging torque reduction).

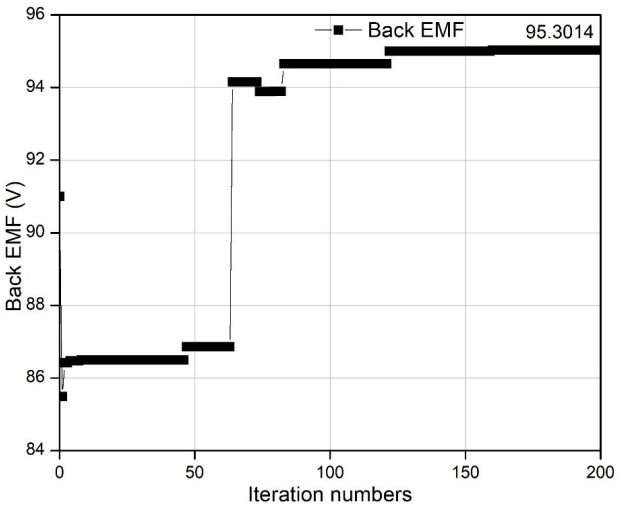

FIGURE 13. Convergence process of objective function (back EMF enhancement).

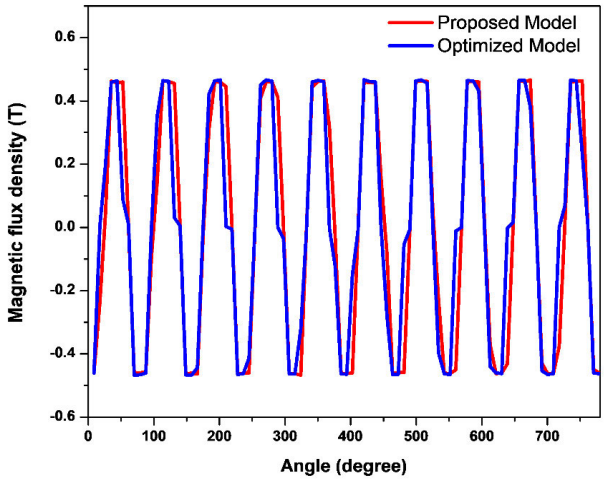

FIGURE 14. Comparison of air gap flux density of proposed and optimized models.

Back EMF after the iterations are 5.23Nm and 95.3014V, respectively.

V. OPTIMIZED MODEL PERFORMANCE ANALYSIS

Comparison of flux density waveform across air gap for proposed and optimized models is presented in Fig. 14. Figure displays that air gap flux density is almost the same for both the models because of the no change in air gap length for both the models.

The flux density distribution plots in the coil region and the overall AFPM machine optimized model is expressed in Fig. 15(a) and Fig. 15(b), correspondingly. The maximum flux density of the optimized model is almost 2.08 T that happens at the rotor core and its coil region has the maximum flux density of 0.6 T. The maximum flux density of the optimized model is less than the conventional and proposed model. However, the average flux density of the optimized model is enhanced because of the optimized magnet shape as shown in the coil region plots of flux density distribution. Due to the increase flux density enhancement, the optimized model has enhanced output torque and back EMF.

The back EMF of the proposed and the optimized models is presented in Fig. 16. The optimized model back EMF is increased by 4.0714 V_{rms} when compared with the proposed model. There is an enhancement of 4.5 % in the V_{rms} of optimized model that is attained by the optimization. The proposed model has back EMF THD of 0.4609 % and the optimized model has 0.4601 %. A decrease in THD from 0.4609 to 0.4601 is attained through the optimized model. Proposed model has reduced back EMF THD as compared to the conventional model because its flux density distribution is more sinusoidal. Back EMF THD of optimized and proposed model is shown in Fig. 17.

The cogging torque waveform of the optimized and the proposed models are displayed in Fig. 18. The cogging torque

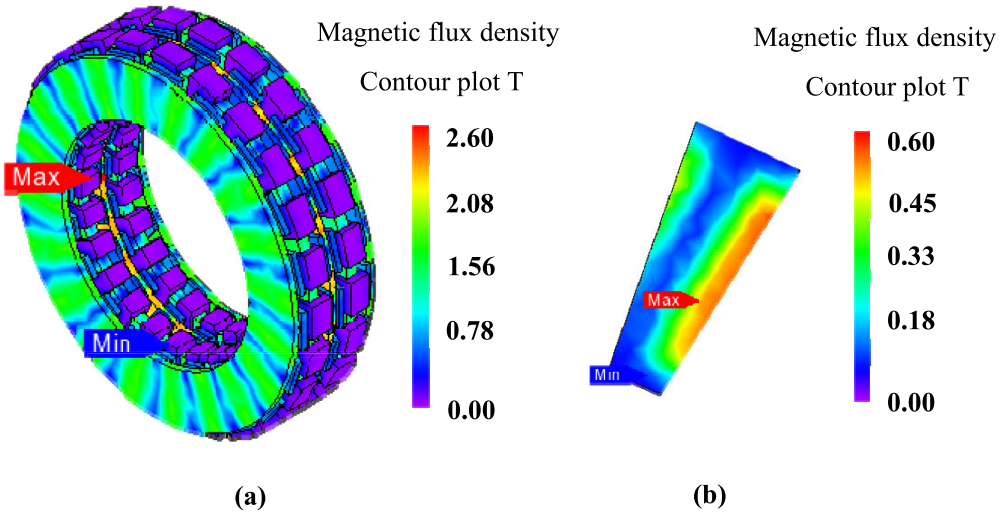

FIGURE 15. Flux density distribution of proposed model: (a) overall model (b) coil region.

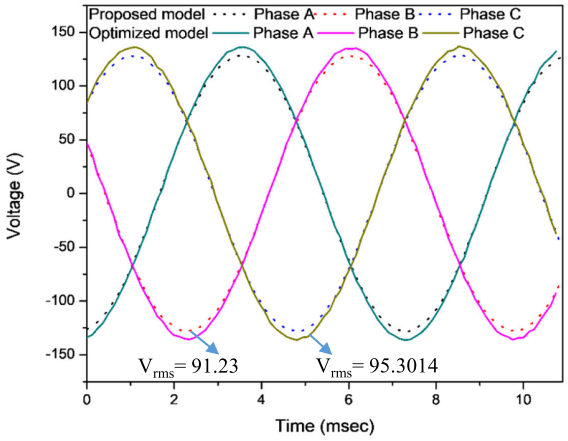

FIGURE 16. Comparison of back EMF of proposed and optimized models.

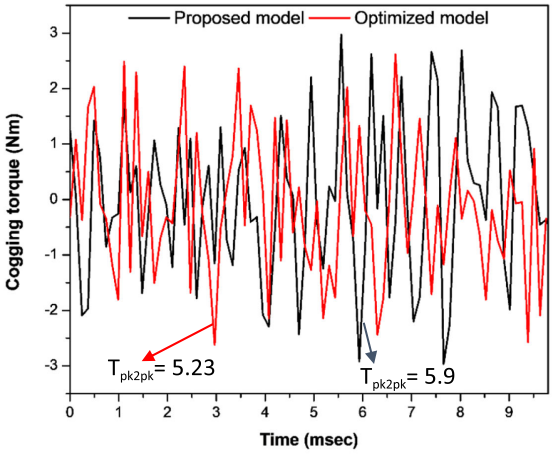

FIGURE 18. Cogging torque comparison of the proposed and optimized models.

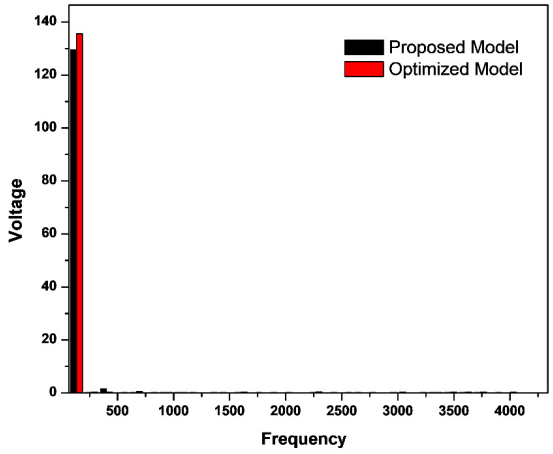

FIGURE 17. Comparison of harmonics of proposed and optimized models.

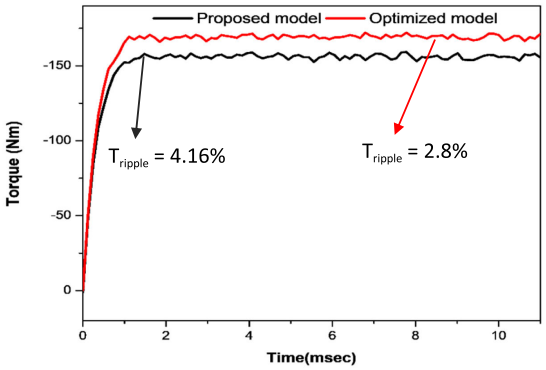

FIGURE 19. Torque comparison of the proposed and optimized models.

is further decreased in the optimized model. The optimized model has an 11.36 % peak to peak decrease in cogging torque as compared to the proposed model.

The output torque comparison of the optimized and proposed models is exhibited in Fig. 19. A significant increase in output torque is accomplished due to optimization. A significant torque ripple reduction is observed in the

TABLE 3. Design parameters of conventional and optimized models.

Parameter	Proposed Model	Optimized Model
X_1	35 mm	33.117 mm
X_2	23 mm	17.728 mm
Total machine axial length	77 mm	77 mm
PM volume	6790.35 mm	6790.35 mm

TABLE 4. Comparison of performance parameters.

Parameter	Units	Proposed Model	Optimized Model
Back EMF	V_{rms}	91.23	95.3014
Output Power	kW	12	13
Torque Ripples	%	4.16	2.8
Average Torque	Nm	151.74	164.491
Cogging Torque Tpk2pk	Nm	5.9	5.2344
B_g (peak-peak)	T	0.92	0.92
VTHD	%	0.4609	0.4601

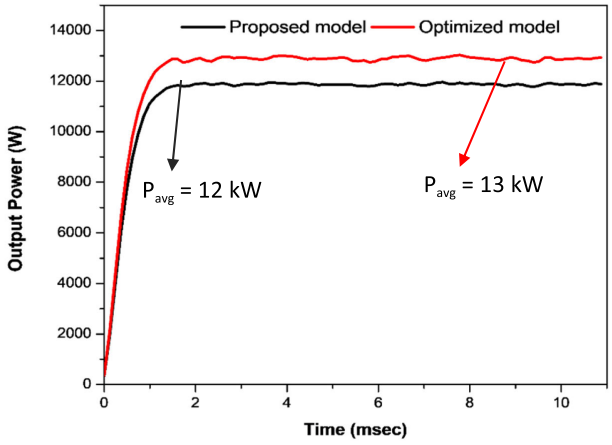

FIGURE 20. Output power comparison of the proposed and optimized models.

optimized model. Average output torque is enhanced by 8.4032 % in the optimized model. A decrease in torque ripple is 32.69 % in the optimized model as compared to the proposed model. Moreover, the output power is increased by 8.33 % in the optimized model as displayed in Fig.20.

The design parameters of proposed and optimized models are presented in Table 3. Magnet volume and axial height are kept fixed for both the optimized model and proposed model. The optimized model has the values of magnet's internal and external widths are 17.728 mm and 33.117 mm, compared to 23 mm and 35 mm for the proposed model, respectively. A quantitative analysis of the different performance parameters is shown in Table 4.

VI. CONCLUSION

The objective was to generate a model of a multi-stack slotless AFPM machine with decreased torque ripples, cogging torque, and better-quality output torque. The configuration chosen for multi-stack AFPM machine is of two stator and three rotors with surface mounted permanent magnets on them. The characteristics analysis is performed by 3D FEA in a multi-stack slot-less AFPM machine. Conventionally in the AFPM machines, the trapezoidal-shaped magnet is utilized. To decrease the torque ripple of AFPM machine right-angled trapezoid permanent magnet is proposed and examined in this paper. The proposed model decreases the torque ripple and cogging torque at the cost of average torque reduction as a comparison to the conventional model. The proposed model optimization is implemented by considering varying inter-polar separation to further increasing the average torque and reducing the cogging torque. The optimized model showed better output performance characteristics compared to the proposed and conventional models.

REFERENCES

[1] G. Xu, G. Liu, W. Zhao, Q. Chen, and X. Du, "Principle of torque-angle approaching in a hybrid rotor permanent-magnet motor," *IEEE Trans. Ind. Electron.*, vol. 66, no. 4, pp. 2580–2591, Apr. 2019.

[2] C. Lopez-Torres, A. Garcia, J.-R. Riba, G. Lux, and L. Romeral, "Computationally efficient design and optimization approach of PMa-SynRM in frequent operating torque–speed range," *IEEE Trans. Energy Convers.*, vol. 33, no. 4, pp. 1776–1786, Dec. 2018.

[3] W. Zhao, A. Ma, J. Ji, X. Chen, and T. Yao, "Multiobjective optimization of a double-side linear Vernier PM motor using response surface method and differential evolution," *IEEE Trans. Ind. Electron.*, vol. 67, no. 1, pp. 80–90, Jan. 2020.

[4] P. Arumugam and C. Gerada, "Short term duty electrical machines," in *Proc. 22nd Int. Conf. Elect. Mach. (ICEM)*, Lausanne, Switzerland, Sep. 2016, pp. 2676–2681.

[5] P. Wannakarn, T. Tanmaneeprasert, N. Rugthaicharoencheep, and S. Nedphograw, "Design and construction of axial flux permanent magnet generator for wind turbine generated DC voltage at rated power 1500 W," in *Proc. 4th Int. Conf. Electr. Utility Deregulation Restructuring Power Technol. (DRPT)*, Weihai, China, Jul. 2011, pp. 763–766.
[6] P. Anpalahan and M. Lamperth, "Design of multi-stack axial flux permanent magnet generator for a hybrid electric vehicle," in *Proc. IEEE Vehicle Power Propuls. Conf.*, Sep. 2006, pp. 1–4.
[7] M. Sadeghiera, A. Darabi, H. Lesani, and H. Monsef, "Design analysis of high-speed axial-flux generator," *Amer. J. Eng. Appl. Sci.*, vol. 1, no. 4, pp. 312–317, Apr. 2008.
[8] F. Sahin, "Design and development of a high-speed axial-flux permanent-magnet machine," Technische Universiteit Eindhoven, Eindhoven, The Netherlands, Tech. Rep., 2001.
[9] C.-T. Liu and S.-C. Lee, "Magnetic field modeling and optimal operational control of a single-side axial-flux permanent magnet motor with center poles," *J. Magn. Magn. Mater.*, vol. 304, no. 1, pp. e454–e456, 2006.
[10] H. Vansompel, P. Sergeant, L. Dupre, and A. Van den Bossche, "Axial flux PM machines with a variable airgap," *IEEE Trans. Ind. Electron.*, vol. 61, no. 2, pp. 730–737, Feb. 2014.
[11] J. M. Davila-Vilchis and R. S. Mishra, "Performance of a hydrokinetic energy system using an axial-flux permanent magnet generator," *Energy*, vol. 65, pp. 631–638, Feb. 2014.
[12] C.-T. Liu, T.-S. Chiang, J. F. D. Zamora, and S.-C. Lin, "Field-oriented control evaluations of a single-sided permanent magnet axial-flux motor for an electric vehicle," *IEEE Trans. Magn.*, vol. 39, no. 5, pp. 3280–3282, Sep. 2003.
[13] J. R. Bumby, R. Martin, M. A. Mueller, E. Spooner, N. L. Brown, and B. J. Chalmers, "Electromagnetic design of axial-flux permanent magnet machines," *IEE Proc. Electr. Power Appl.*, vol. 151, no. 2, pp. 151–160, Mar. 2004.
[14] R. L. Ficheux, F. Caricchi, F. Crescimbini, and O. Honorati, "Axial-flux permanent-magnet motor for direct-drive elevator systems without machine room," *IEEE Trans. Ind. Appl.*, vol. 37, no. 6, pp. 1693–1701, 2001.
[15] C. Liu, J. Lu, Y. Wang, G. Lei, J. Zhu, and Y. Guo, "Techniques for reduction of the cogging torque in claw pole machines with SMC cores," *Energies*, vol. 10, p. 1541, Oct. 2017.
[16] N. S., S. P. Nikam, S. Pal, A. K. Wankhede, and B. G. Fernandes, "Performance comparison between PCB-stator and laminated-core-stator-based designs of axial flux permanent magnet motors for high-speed low-power applications," *IEEE Trans. Ind. Electron.*, vol. 67, no. 7, pp. 5269–5277, Jul. 2020.
[17] M. G. Kesgin, P. Han, N. Taran, and D. M. Ionel, "Overview of flywheel systems for renewable energy storage with a design study for high-speed axial-flux permanent-magnet machines," in *Proc. 8th Int. Conf. Renew. Energy Res. Appl. (ICRERA)*, Brasov, Romania, Nov. 2019, pp. 1026–1031.
[18] W. J. Cheng, Z. Deng, L. Xiao, B. Zhong, and Y. Sun, "An analytical solution to the electromagnetic performance of an ultra-high-speed PM motor," *J. Electr. Comput. Eng.*, vol. 2019, Sep. 2019, Art. no. 1469637.
[19] S. Kumar, W. Zhao, Z. S. Du, T. A. Lipo, and B.-I. Kwon, "Design of ultrahigh speed axial-flux permanent magnet machine with sinusoidal back EMF for energy storage application," *IEEE Trans. Magn.*, vol. 51, no. 11, Nov. 2015, Art. no. 8113904.
[20] S. Kumar, T. A. Lipo, and B.-I. Kwon, "A 32 000 r/min axial flux permanent magnet machine for energy storage with mechanical stress analysis," *IEEE Trans. Magn.*, vol. 52, no. 7, Jul. 2016, Art. no. 8205004.
[21] Y. Liu, Z. Zhang, C. Wang, W. Geng, and T. Yang, "Design and analysis of oil-immersed cooling stator with nonoverlapping concentrated winding for high-power ironless stator axial-flux permanent magnet machines," *IEEE Trans. Ind. Electron.*, vol. 68, no. 4, pp. 2876–2886, Apr. 2021.
[22] P. Liang, F. Chai, L. Chen, and Y. Wang, "Analytical prediction of no-load stator iron losses in spoke-type permanent-magnet synchronous machines," *IEEE Trans. Energy Convers.*, vol. 33, no. 1, pp. 252–259, Mar. 2018.
[23] P. Liang, F. Chai, Y. Yu, and L. Chen, "Analytical model of a spoke-type permanent magnet synchronous in-wheel motor with trapezoid magnet accounting for tooth saturation," *IEEE Trans. Ind. Electron.*, vol. 66, no. 2, pp. 1162–1171, Feb. 2019.
[24] Y.-X. Liu, J.-W. Cao, Q.-H. Gao, Z.-H. Liu, Y.-C. Lu, and Z.-Y. Sun, "Electromagnetic performance of the novel hybrid-pole permanent magnet machines for high peak torque density," *IEEE Access*, vol. 8, pp. 220384–220393, 2020.
[25] C.-C. Hwang, P.-L. Li, F. C. Chuang, C.-T. Liu, and K.-H. Huang, "Optimization for reduction of torque ripple in an axial flux permanent magnet machine," *IEEE Trans. Magn.*, vol. 45, no. 3, pp. 1760–1763, Mar. 2009.
[26] M. Shokri, N. Rostami, V. Behjat, J. Pyrhonen, and M. Rostami, "Comparison of performance characteristics of axial-flux permanent-magnet synchronous machine with different magnet shapes," *IEEE Trans. Magn.*, vol. 51, no. 12, pp. 1–6, Dec. 2015.
[27] T. Labbé, B. Dehez, M. Markovic, and Y. Perriard, "Torque-to-weight ratio maximization in PMSM using topology optimization," in *Proc. 19th Int. Conf. Elect. Mach.*, Rome, Italy, Sep. 2010, pp. 1–5.
[28] T. J. E. Miller, "Advanced theory and modern applications of Brushless permanent magnet motors," Sogo Electron. Press, Tokyo, Japan, Tech. Rep., 2003.
[29] S. A. Evans, "Salient pole shoe shapes of interior permanent magnet synchronous machines," in *Proc. 19th Int. Conf. Electr. Mach. (ICEM)*, Rome, Italy, Sep. 2010, pp. 1–6.
[30] J. F. Gieras, R. J. Wang, and M. J. Kamper, *Axial Flux Permanent Magnet Brushless Machines*. Dordrecht, The Netherlands: Kluwer, 2008, pp. 45–60 and 92–119.
[31] L. Dosiek and P. Pillay, "Cogging torque reduction in permanent magnet machines," *IEEE Trans. Ind. Appl.*, vol. 43, no. 6, pp. 1565–1571, Nov. 2007.
[32] P. Irasari, M. Kasim, M. Hikmawan, P. Widiyanto, K. Wirtayasa, and Q. M. B. Soesanto, "Optimization of modular stator construction to improve permanent magnet generator characteristics for very low head hydro power application," in *Proc. Int. Conf. Sustain. Energy Eng. Appl. (ICSEEA)*, Jakarta, Indonesia, Oct. 2017, pp. 1–8.
[33] M. Aakif Baig, J. Ikram, A. Iftikhar, S. S. H. Bukhari, N. Khan, and J.-S. Ro, "Minimization of cogging torque in axial field flux switching machine using arc shaped triangular magnets," *IEEE Access*, vol. 8, pp. 227193–227201, 2020.
[34] Z. S. Du and T. A. Lipo, "Reducing torque ripple using axial pole shaping in interior permanent magnet machines," *IEEE Trans. Ind. Appl.*, vol. 56, no. 1, pp. 148–157, Jan. 2020.
[35] *PIAnO Introduction*. Accessed: Apr. 1, 2018. [Online]. Available: http://pidotech.com/en/product/piano.aspx
[36] W. Chai, T. Lipo, and B.-I. Kwon, "Design and optimization of a novel wound field synchronous machine for torque performance enhancement," *Energies*, vol. 11, no. 8, p. 2111, Aug. 2018.
[37] M. Nikouie, O. Wallmark, and L. Harnefors, "Torque-ripple minimization for permanent-magnet synchronous motors based on harmonic flux estimation," in *Proc. 20th Eur. Conf. Power Electron. Appl.*, Riga, Latvia, 2018, pp. 1–8.

MUHAMMAD YOUSUF received the B.S. degree in electrical engineering (electronics) from the Federal Urdu University of Arts Science and Technology (FUUAST) Islamabad, Pakistan, in 2015, and the M.S. degree in electrical engineering from COMSATS University Islamabad, (Abbottabad Campus), Abbottabad, Pakistan, in 2019, where he is currently pursuing the Ph.D. degree in electrical engineering. His research interests include design, analysis, and optimization of permanent magnet flux switching machines, linear flux switching machines, and axial flux permanent magnet machines.

FAISAL KHAN (Member, IEEE) received the B.S. degree in electronics engineering and the M.S. degree in electrical engineering from COMSATS University Islamabad, Abbottabad Campus, Pakistan, in 2009 and 2012, respectively, and the Ph.D. degree in electrical engineering from Universiti Tun Hussein Onn Malaysia, Malaysia, in 2017. From 2010 to 2012, he was a Lecturer with the University of Engineering and Technology, Abbottabad, Pakistan. Since 2017, he has been an Assistant Professor with the Electrical and Computer Engineering Department, COMSATS University Islamabad (Abbottabad Campus), Pakistan. He is the author of more than 100 publications, two patents, and has received multiple research awards. His research interests include design of flux-switching, synchronous and DC machines. Furthermore, he is a member of IEEE Industrial Electronics Society and IEEE-IES Electrical Machines Technical Committee.

JUNAID IKRAM received the B.E. degree in electrical engineering from the University of Engineering and Technology Lahore, Pakistan, in 2005, the M.S. degree from Hanyang University, South Korea, in 2009, and the Ph.D. degree in electrical engineering from Comsats University Islamabad, Pakistan, in 2017. He is currently working as a Senior Engineer in COMSATS University Islamabad. His research interests include design, analysis, and optimization of axial flux machines, vernier machines, wound rotor synchronous machine, hybrid flux switching machines, and modeling of the machine losses.

RABIAH BADAR received the M.S. degree in computer engineering and the Ph.D. degree in electrical engineering from COMSATS University, Islamabad, in 2007 and 2009, respectively. From February 2015 to May 2015, she was with the Namal College, Mianwali, Pakistan, as an Assistant Professor. After that, she joined COMSATS University, Islamabad, as an Assistant Professor. She served as a pioneer Incharge of BS Electrical (Power) Engineering program. She is the author of many international, peer reviewed journal research articles, conference papers, and book chapters. She has successfully supervised many undergraduate and graduate research thesis. Her research interests include artificial intelligence, optimization, soft computing, power system stability and control, nonlinear adaptive control, FACTS, HVDC, and renewable energy systems.

SYED SABIR HUSSAIN BUKHARI (Member, IEEE) received the B.E. degree in electrical engineering from the Mehran University of Engineering and Technology Jamshoro, Pakistan, in 2009, and the Ph.D. degree from the Department of Electronic Systems Engineering, Hanyang University, South Korea, in 2017. He joined Sukkur IBA University as an Assistant Professor, in December 2016. He is currently working as a Research Professor with Chung-Ang University, Seoul, South Korea, under Korean Research Fellowship (KRF) Program. His main research interests include electric machine design, power quality, and drive controls.

JONG-SUK RO received the B.S. degree in mechanical engineering from Han-Yang University, Seoul, South Korea, in 2001, and the Ph.D. degree in electrical engineering from Seoul National University (SNU), Seoul, South Korea, in 2008. He conducted research at the Research and Development Center, Samsung Electronics, as a Senior Engineer, from 2008 to 2012. From 2012 to 2013, he was with the Brain Korea 21 Information Technology of SNU, as a Postdoctoral Fellow. He conducted research at the Electrical Energy Conversion System Research Division, Korea Electrical Engineering and Science Research Institute, as a Researcher, in 2013. From 2013 to 2016, he worked with the Brain Korea 21 Plus, SNU, as a BK Assistant Professor. In 2014, he was with the University of Bath, Bath, U.K. He is currently an Associate Professor with the School of Electrical and Electronics Engineering, Chung-Ang University, Seoul, South Korea. His research interests include the analysis and optimal design of next-generation electrical machines using smart materials such as electromagnet, piezoelectric, magnetic shape memory alloy, and so on.